Electrochimica Acta 112 (2013) 943–949

Contents lists available at ScienceDirect

Electrochimica Acta

journal homepage: www.elsevier.com/locate/electacta

Mass transport in electrochemical nanogap sensors

Klaus Mathwig, Serge G. Lemay*

MESA+Institute for Nanotechnology, University of Twente, PO Box 217, 7500 AE Enschede, The Netherlands

ARTICLE INFO

Article history:
Received 1 October 2012
Received in revised form 25 May 2013
Accepted 27 May 2013
Available online 18 June 2013

Keywords:
Electrochemical sensor
Mass transport
Finite-element methods
Redox cycling
Nanofluidics

ABSTRACT

Nanofluidic thin-layer cells based on redox cycling allow for extremely sensitive electrochemical detection. Here we establish a physical mass-transfer model for analyte molecules in these transducers which takes into account advective and diffusive transport of both oxidized and reduced species as well as reversible dynamic adsorption at the sensor surfaces. We use finite-element modeling to determine the transient response of nanogap sensors; numerically we predict that the response time can be reduced substantially by pressure-driven advection while the faradaic limiting current remains unaffected by this flow for all experimentally accessible flow rates.

1. Introduction

Electrochemical nanogap sensors are based on the repeated oxidation and reduction of redox active molecules at closely spaced ($\ll$1 μm) electrodes embedded in the bottom and ceiling of a nanochannel. The analyte molecules diffuse back and forth and thus shuttle thousands of electrons from one electrode to the other, thereby generating such a highly amplified current that even electrochemical detection of single molecules becomes possible [1,2]. A schematic of a nanogap sensor and a micrograph of a typical device are shown in Fig. 1.

Our group has recently reported on several experimental properties of nanogap devices, in particular:

1. As opposed to ultramicroelectrodes [3,4], the faradaic limiting current is unaffected by advective flow at the device surface [5] (e.g., when the device is embedded in a larger microchannel for lab-on-a-chip applications). The small nanochannel cross section imposes a large hydraulic resistance on any flow generation in the channel, and mass transport between the electrodes thereby remains diffusion-limited at all times. This gives these devices the intrinsic advantage of performing a concentration measurement that does not require calibration for varying flow rates, i.e., changing advective mass transport to the electrodes.
2. The large surface to volume ratio of the nanochannel of approximately $2 \times 10^7 m^{-1}$ leads to a pronounced adsorption of analyte molecules [2,6]. Typically, this dynamic adsorption is reversible and occurs on time scales much more rapid than those probed in sensing experiments. In this case adsorption can be quantified in terms of a surface concentration of adsorbed analytes or, more conveniently for quantifying its impact on device performance, in terms of the ratio of dissolved and adsorbed molecules.
3. The response time of the nanosensors after a change in concentration at the inlet is determined by diffusive transport of molecules into or out of the device to equilibrate with the concentration in the bulk reservoir. This equilibration is slowed down considerably by adsorption, a factor ~10 increase in the response time being typical even for well-behaved outer sphere reactions [7].
4. Instead of coupling a nanogap sensor purely diffusively to a bulk reservoir, molecules can be actively transported into the transducer by using a syringe pump to generate a pressure difference in between the two access holes at both ends of the nanochannel [8,9]. At high pump flow rates, this advective transport is considerably faster than longitudinal diffusion in the channel.

In this paper we state the governing equations for continuum transport of the two species of a redox couple and model time-dependent transport and adsorption using two-dimensional finite-element analysis. In particular, we show how advective flow along the nanochannel can greatly enhance the response speed of electrochemical nanogap transducers.

2. Physical model

A schematic of transport in a nanogap sensor of height h is shown in Fig. 2. For definiteness and without loss of generality, we

* Corresponding author. Tel.: +31 53 489 2306.
E-mail addresses: k.h.mathwig@utwente.nl (K. Mathwig), s.g.lemay@utwente.nl (S.G. Lemay).

0013-4686/$ – see front matter © 2013 Elsevier Ltd. All rights reserved.
http://dx.doi.org/10.1016/j.electacta.2013.05.142

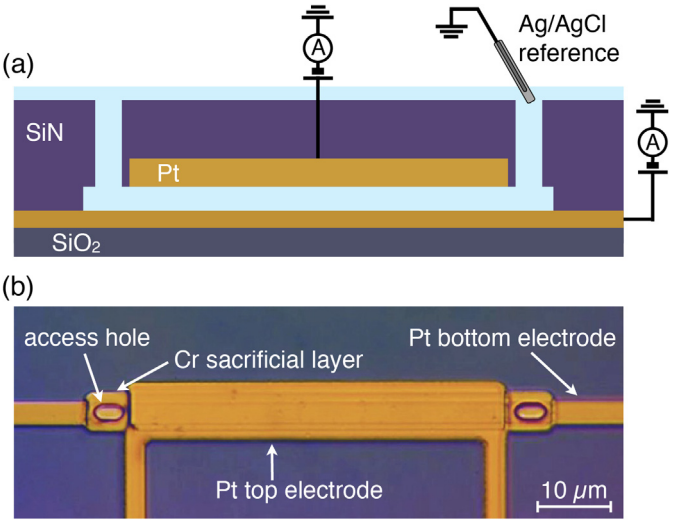

Fig. 1. (a) Schematic cross section of a nanogap sensor. Redox-active molecules shuttle diffusively between the closely spaced (~100 nm) Pt electrodes, where they are repeatedly oxidized and reduced and generate a highly amplified electrochemical current. (b) Optical micrograph (top view) of a device consisting of a 50 μm long and 5 μm wide detection region. The solution-filled nanochannel is originally defined by a sacrificial Cr layer, which is wet etched immediately prior to electrochemical measurements.

consider the case where analyte molecules are oxidized at a bottom electrode and reduced at the opposing top electrode, both electrodes being of equal length L. The molecules are transported by diffusion and longitudinal advection and can adsorb reversibly and dynamically at the electrode surfaces. Only the reduced species is transported into the active area by advection (from the left) and diffusion. The x and z axes correspond to the longitudinal axis of the nanochannel and the direction perpendicular to the electrodes, respectively, as shown in Fig. 2. It is further assumed that the nanochannel is bound laterally by vertical insulating walls such that its width w is much greater than its height h, and that the electrodes span the full width of the channel. Under these conditions, the transport properties are essentially independent of the y coordinate.

A general, comprehensive model for coupled mass transport and surface reactions in microfluidic systems is given by Gervais and Jensen [10] for one analyte species and a Langmuir adsorption isotherm. Here we adapt this model to our nanofluidic system with two species, namely, the reduced and oxidized forms of the analyte. In a continuum description, the mass transport of a concentration of

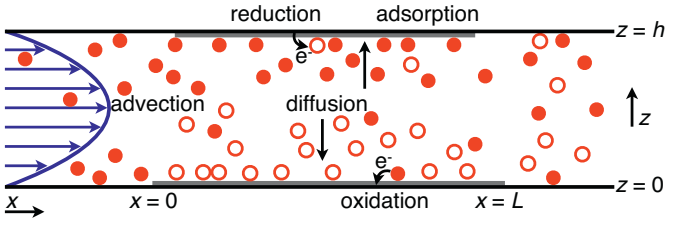

Fig. 2. Schematic of transport of analyte molecules in a nanogap sensor. The channel is coupled to a reservoir with an inflow with an initial concentration of reduced molecules c_{red} from the left and an outlet to the right. Molecules are transported by a superposition of advection and diffusion. They are oxidized at the bottom electrode and reduced at the top electrode and adsorb reversibly at both surfaces. Note the highly skewed geometry: a typical is channel h = 50–200 nm high while the electrodes have a length of L = 10–100 μm.

reduced and oxidized molecules $c_{red,ox}$ is governed by the transport equations

$$\frac{\partial c_{red}}{\partial t} = -\nabla \cdot \mathbf{N}_{red}, \quad \frac{\partial c_{ox}}{\partial t} = -\nabla \cdot \mathbf{N}_{ox}, \tag{1}$$

with the diffusive and advective molar fluxes **N** being given by

$$\mathbf{N}_{red} = -D \cdot \nabla c_{red} + \mathbf{u}\, c_{red}, \quad \mathbf{N}_{ox} = -D \cdot \nabla c_{ox} + \mathbf{u} c_{ox}. \tag{2}$$

Here **u** is the liquid velocity profile in the nanochannel and D is the diffusion coefficient. We approximate identical diffusion coefficients for both species and do not consider bulk reactions in the channel or migration in an electric field; experimentally a high supporting electrolyte concentration confines any such field to a Debye layer of extent ≤1 nm.

Transport of the molecules adsorbed at each electrode surface, with surface concentration c_s, is governed by

$$\frac{\partial c_s}{\partial t} = R_{ads} - R_{des}, \tag{3}$$

where R_{ads} and R_{des} are rates of adsorption and desorption, respectively. The comparatively small contribution from surface diffusion is neglected.

Surface and bulk concentrations are coupled by flux equilibria at the surfaces, which further encode the electrochemical reactions taking place at the electrodes. We only examine the case of a high electrochemical overpotential, i.e., *all* reduced molecules impinging on the bottom electrode undergo oxidation and all oxidized molecules are consumed at the reducing top electrode (fast electron-transfer kinetics are thus implicitly assumed). This case represents by far the most common configuration for detection experiments. Under these conditions, the concentration of reduced molecules at the oxidizing surface at z = 0 is diminished to zero, while the same occurs for the oxidized species at the opposing reducing electrode located at $z = h$:

$$c_{red}|_{z=0} = 0, \quad c_{ox}|_{z=h} = 0. \tag{4}$$

At the oxidizing bottom electrode, an inward normal flux $N_{n,ox}$ of oxidized molecules is generated. This flux is equal and opposite to the normal gradient of the reduced molecules being consumed, minus the net ad/-desorption $R_{ads} - R_{des}$ at the electrode surface. The exact opposite behavior is taking place at the bottom electrode:

$$\begin{aligned} N_{n,ox}|_{z=0} &= -D \cdot \nabla_n c_{red} - (R_{ads} - R_{des}), \\ N_{n,red}|_{z=h} &= -D \cdot \nabla_n c_{ox} - (R_{ads} - R_{des}). \end{aligned} \tag{5}$$

For simplicity we also assume that reversible adsorption in the devices follows a linear Freundlich adsorption isotherm, i.e., the number of adsorption sites is virtually unlimited and the surface never saturates (at the experimentally investigated analyte concentrations of up to 1 mM). Therefore the rates are expressed by

$$R_{ads} = k_{on} c_w, \quad R_{des} = k_{off} c_s. \tag{6}$$

Here k_{on} and k_{off} are constants of adsorption and desorption and c_w is the analyte concentration near the surface in the bulk channel.

Nanoscale sensors also exhibit stochastic behavior [8,11]: Brownian motion leads to a pronounced number density fluctuation of molecules in the small detection volume. This is reflected in fluctuations of the detected faradaic current. Naturally these stochastic fluctuations are not captured by the *continuum* model presented here. The relative fluctuations scale with $c^{-1/2}$; for a typical 10 fL detection volume and 1 mM analyte concentration the faradaic current exhibits an rms 'noise' of only 0.03%. But the relative fluctuations increase to 10% for a 10 nM concentration. A stochastic transport model is discussed in [12].

3. Relevant transport regime

The general physical model introduced above describes a vast range of situations depending on the relative values of the physical parameters characterizing the particular system of interest. Since our aim is to describe the properties of experimentally realizable nanogap sensors, physical understanding of the mass transport processes at play can be greatly improved by identifying which regime is dominant in this specific situation. This in particular helps to contrast with previously studied cases such as protein binding in nanochannels [13,14].

Typical redox-active analytes include ferricyanide, ruthenium hexamine and ferrocene derivatives in aqueous solution (but also organic solvents) at high supporting electrolyte concentrations (e.g. 0.1–1 M KCl). These analytes exhibit diffusivities of about $D = 5 \times 10^{-10}$ m^2/s and fast electron transfer kinetics. For ferrocenedimethanol in 2 M aqueous KCl, a high heterogenous rate constant of k_0 =10 cm/s was determined in a nanogap sensor [15]. This is fast compared to the 'rate' of diffusion across the nanochannel of $2D/h = 1$ cm/s for $h = 100$ nm and therefore diffusion-limited transport is ensured even at modest overpotentials. Comparably fast kinetics have also be determined for other compounds such as $k_0 = 17$ cm/s for ruthenium hexamine [16] or $k_0 = 5$ cm/s for ferrocenylmethyltrimethylammonium [17]. Generally nanogap sensors can be characterized by large surface Damköhler numbers of Da $= k_0 h/D > 1$.

3.1. Fluid transport

When liquid is driven through the nanogap device [8] by a pressure difference Δp, the hydraulic resistance R_{hyd} of the nanochannel opposes any flow Q according to Poiseuille's law $Q = \Delta p/R_{\mathrm{hyd}}$. For a channel with a rectangular cross section, the resistance is given by [18]

$$R_{\mathrm{hyd}} \approx \frac{12\eta L}{1 - 0.63(h/w)} \frac{1}{h^3 w} \quad \text{for } h < w, \tag{7}$$

with η being the dynamic viscosity of 0.001 Pa s for aqueous solutions. Resistances range from $R_{\mathrm{hyd}} = 3 \times 10^{18}$ Pa s m^{-3} for a device with the geometry $h = 200$ nm, $w = 5$ μm, $L = 10$ μm to $R_{\mathrm{hyd}} = 2 \times 10^{21}$ Pa s m^{-3} for $h = 50$ nm, $w = 5$ μm, $L = 100$ μm. Therefore, to drive maximal mean flow velocities of $U = Q/wh < 1$ mm/s, a pressure gradient of $\Delta p = 3$–500 kPa has to be applied along the nanochannel. The maximal pressure that is accessible experimentally is typically limited to approximately 100 kPa by leakage in microfluidic feed lines. The slow flow leads to very small Reynolds numbers $\mathrm{Re} = \rho U h/\eta < 10^{-4}$, where ρ is the water density of 1000 kg m^{-3}. Therefore, flow is always fully developed and a laminar flow profile is established with the parabolic shape

$$\mathbf{u} = (u_x, u_y, u_z) = \left(\frac{3}{2} U \left[1 - \left(\frac{z - h/2}{h/2} \right)^2 \right], 0, 0 \right). \tag{8}$$

Because of the comparatively wide channel and the corresponding large lateral aspect ratio of $w/h \geq 50$, any lateral forces and gradients can be neglected to a good approximation and the problem is reduced to two dimensions.

3.2. Analyte transport

Due to the limited advection velocity and short vertical diffusion path, transport takes place in a regime of low surface Péclet numbers Pe. This number relates the time for vertical diffusion of a distance h across the channel to time for longitudinal convection along the same distance. For the diffusion coefficient $D = 5 \times 10^{-10}$ m^2/s typical of small redox molecules, $\mathrm{Pe} = Uh/D < 0.4$ for the values of U and h introduced above. This means that molecules in solution sample the channel cross section homogenously, no Taylor dispersion takes place, and the advective velocity U also describes the average velocity experienced by each individual molecule passing through the channel [8]. Furthermore, transport on the length scale h being dominated by diffusion, the linear concentration profile across the channel that is typical for thin-layer cells [15,19] is not influenced significantly by flow. That is, the concentration of each species increases *linearly* from zero at the respective consuming electrode to a maximal level at the generating electrode, as will be observed explicitly in Fig. 4.

Another direct consequence of the low Pe numbers, coupled with the long channel length L, is that analyte molecules are transported in a regime of small Graetz numbers Gz = Pe $h/L = Uh^2/(LD) < 0.008$. Gz compares advection along the nanochannel length L to vertical diffusion. In this fully developed regime, all molecules are advected through the sensor slowly enough that they are able to diffuse to the surfaces and no surface boundary layer can develop.

3.3. Adsorption

Intrinsic to nanofluidic devices is a very high surface-to-volume ratio of $2h^{-1} = 1$–5×10^7 m^{-1}. This leads to a pronounced adsorption of molecules on the nanochannel walls. The adsorption does not influence electron transfer and is reversible on a timescale which is too short to be accessible experimentally at present. Therefore, it is simply described by the ratio of the number of molecules in solution N_{sol} to adsorbed molecules N_{ads} of typically $\varepsilon = N_{\mathrm{sol}}/N_{\mathrm{ads}} = 0.1$–1 (depending on channel height and specific adsorptivity) [6,7], corresponding to a surface concentration of $c_S = 50$ fmol mm^{-2} for $\varepsilon = 1$ and $h = 100$ nm.[1]

While ε can be experimentally determined in situ by stochastic amperometry [6], the mechanism and kinetics of adsorption are not well understood. Nonetheless, it is possible to estimate upper limits for the rates of ad- and desorption and to determine their ratio. For simplicity, we assume diffusion-limited adsorption, i.e., c_S and molecules in solution in the nanochannel are always in equilibrium *locally*. This means that all molecules desorb on a time scale shorter than the time it takes to diffuse through the channel vertically: $t < h^2/(2D) = 10$ μs. The corresponding lower limit for k_{off} is $k_{\mathrm{off}} = 1/t = 10^5$ s^{-1}. An adsorption constant of $k_{\mathrm{on}} > 5$ mm/s is then determined from the steady state equilibrium $k_{\mathrm{on}} c_w = k_{\mathrm{off}} c_S$ or, equivalently, $2\, k_{\mathrm{on}} \varepsilon = h\, k_{\mathrm{off}}$.[2]

3.4. Steady state propagation velocity

Since analyte molecules are immobilized for part of the transit time through the sensor, dynamic adsorption leads to retardation of these molecules' average velocity with respect to the liquid flow [8,10].

In steady state, this mean propagation velocity U_{eff} is reduced to

$$U_{\mathrm{eff}} = \left(1 - \frac{N_{\mathrm{ads}}}{N_{\mathrm{ads}} + N_{\mathrm{sol}}} \right) U = \frac{\varepsilon\, U}{\varepsilon + 1}. \tag{9}$$

Longitudinal diffusive transport is effectively slowed down by the same exact retardation factor.

[1] $c_S = 50$ fmol mm^{-2} is comparable to typical surface concentrations encountered in microfluidic protein immunoassays or fluidic microresonators [10].

[2] More precisely, the time scale is set by the slowest of either the ad- or desorption process: $h^2/(2D) > (k_{\mathrm{on}}/h + k_{\mathrm{off}})^{-1}$. In experiments the desorption term k_{off} is found to be dominant.

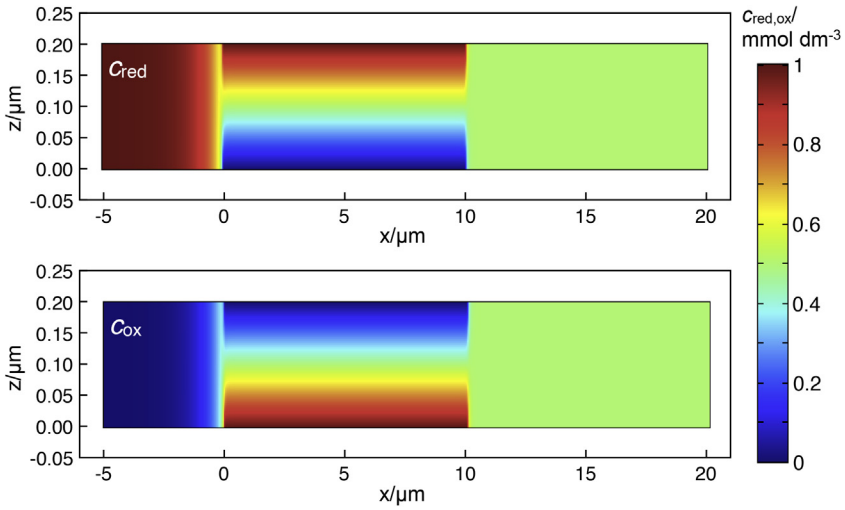

Fig. 3. Finite-element simulation of the steady state bulk concentrations c_{red} and c_{ox} with $D = 5 \times 10^{-10}$ m^2/s for an inflow of c_{red} =1 mM at U = 500 µm/s from the left. A reducing top electrode and a corresponding oxidizing bottom electrode are positioned at x = 0–10 µm. The active region has a high aspect ratio of 1:50; for clarity of presentation, the vertical scale has been expanded here.

4. Numerical results

We employ finite element analysis (COMSOL Multiphysics 4.2) in two dimensions to study the transient response of a nanogap sensor to a concentration change using the differential equations and boundary conditions Eqs. (1)–(6). We employ realistic experimental values instead of scaled dimensionless equations in order to facilitate comparison to physically realizable experimental situations. As shown in Fig. 3, we simulate a 25 µm long and 200 nm high nanochannel with a 10 µm long active region between top and bottom electrodes of equal length. This is a conservative geometry as a longer and shallower channel would exhibit smaller Reynolds, surface Péclet and Graetz numbers, further strengthening the trends reported here. As initial conditions, the whole geometry is filled exclusively with reduced molecules c_{red} = 1mM of $D = 5 \times 10^{-10}$ m^2/s, while no molecules are adsorbed at any surface. The same solution enters the geometry from the left with the flow profile Eq. (8) while the right boundary serves as outlet.

In Fig. 3 the steady-state concentrations of reduced and oxidized molecules are shown for a flow velocity U = 500 µm/s. For this simulation a fast adsorption constant k_{on} = 0.1 m/s and ε = 1 is used, so that the number of adsorbed molecules in the steady-state becomes equal to the number of molecules in solution in the detection area. The entrance region $x = -5$ to 0 µm is filled exclusively with reduced molecules, reflecting the composition of the injected solution. In the active segment, c_{red} changes linearly between a maximum concentration at the top (reducing) electrode to zero at the bottom (oxidizing) electrode. In the outlet region to the right, the solution contains equal concentrations of reduced and oxidized species, reflecting the relative concentrations of the two species in the active region of the device. Throughout the whole simulation domain, the concentration of oxidized species is complementary to that of the reduced species, $c_{ox} = 1\,\text{mM} - c_{red}$ (in steady state), reflecting the symmetry of Eqs. (1)–(6), while c_S is constant along the electrodes.

Experimentally, the time response of nanogap sensors is most conveniently measured by exploiting the fact that adsorption to an electrode depends on applied potential [7]. By stepping the potential, analyte molecules can be instantaneously depleted from or accumulated in the active region. This temporary departure from steady-state conditions occurs only in the liquid plug located in the active region $x = 0 \ldots L$, and the transient response is

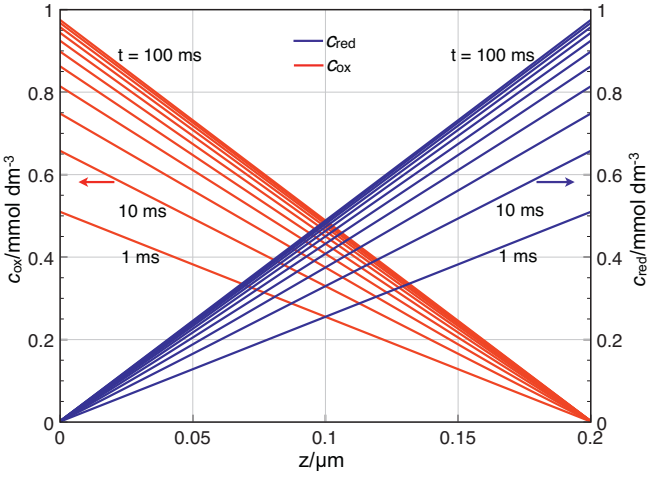

Fig. 4. Concentration profiles c_{red} and c_{ox} across the channel as a function of time evaluated at the center of the device at x = 5 µm for the geometry shown in Fig. 3 and in the Supporting Movie. Starting conditions at t = 0 s are c_{red} = 1mol m^{-3}, c_S = 0 mol m^{-2} and c_{ox} = 0 mol m^{-3}. Eleven times t = 1 ms, 10 ms, 20 ms, 30 ms . . .100 ms are shown as liquid is advected into the device at U = 667 µm/s. Already within the first millisecond of the simulation, a local equilibrium of adsorbed and dissolved molecules is established, i.e., half of the molecules adsorb and the bulk nanochannel is depleted.

monitored via the faradaic current as the concentration equilibrates once again with the reservoir. Setting the surface concentration c_S = 0 as initial condition, as described above, represents the equivalent situation in the simulations and facilitates comparison with experiments.

The time-dependent concentration change of c_{red} is shown in the Supporting Information in the form of a movie[3] for a flow velocity of U = 667µm/s. The corresponding concentration profiles $c_{red,ox}$ across the channel at x = 5 µm (the center of the active region) are shown in Fig. 4 at specific moments in time. As

[3] The Supplementary Movie shows the change in c_{red} for the geometries shown in Figs. 3 and 4. Starting conditions are a constant analyte concentration c_{red} throughout the geometry and c_S = 0 mM, which leads to instant depletion in the detection area to 0.5 c_{red}. The concentration in solution is then brought into equilibrium by an inflow of U = 667 µm/s. 1 ms long timesteps ranging from t = 0 . .0.15s are shown.

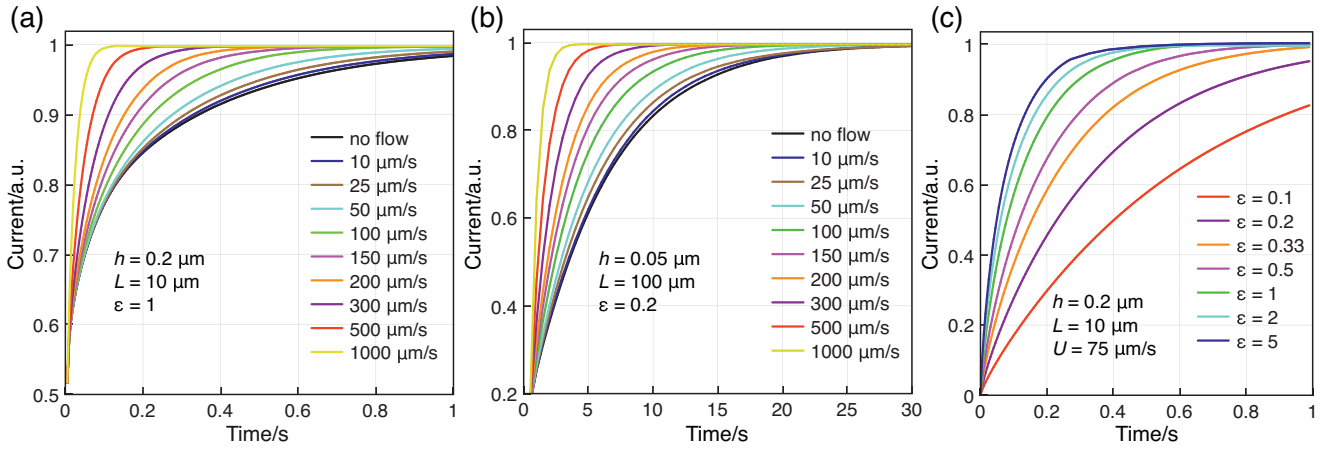

Fig. 5. Transient response as a function of advective flow velocity and adsorption fraction. (a) Transients in a device of the standard geometry $h = 0.2$ µm, $L = 10$ µm and an adsorption fraction $\varepsilon = 1$. Mean flow velocities are varied up to $U = 1000$ µm/s. (b) Response in a 100 µm long and 0.5 µm high geometry. Note that the time scale is increased by a factor of 30 compared to (a). (c) Transients in the standard geometry as a function of the adsorption fraction at a flow velocity $U = 75$ µm/s.

expected, the simulation shows that quasi-steady-state conditions for adsorption and mass transport in the z-direction are achieved almost instantaneously. After a minimal time interval of only 1 ms, linear concentration profiles are fully established across the channel, reflecting the low Pe number. The concentrations range from 0 mM to 0.5 mM, thereby depleting the overall analyte concentration in the channel to 50% of that in the bulk. Correspondingly, half of the molecules originally in the active region are now adsorbed at the surfaces, as expected for $\varepsilon = 1$ (c_S is not shown in plot). The concentration profile then evolves gradually as the bulk and surface concentrations increase under the influence of an inflow of 1 mM c_{red} at $U = 667$ µm/s from the left, asymptotically establishing the limiting steady-state concentration profiles. Notably, this equilibration is slowed down by the adsorption of molecules as they move into the sensor, and it takes approximately 100 ms before settling fully, much longer than the liquid transit time through the active region of 20 ms.

Experimentally the transient response is determined as a faradaic electrical current–time trace $I(t)$ recorded at either electrode. This response is directly proportional to the concentration of molecules in solution in the transducer and can be extracted from the simulations through

$$I(t) = \pm n F w \int_{x=0}^{x=L} D \cdot \nabla_n c_{red,ox}(t)\, dx\,|_{z=0,h} \qquad (10)$$

(F: Faraday constant, n: number of electrons per charge transfer).

The simulated transients $I(t)$ are shown in Fig. 5a for flow velocities ranging from zero to $U = 1000$ µm/s. As for the purely diffusive case, the transients' shape resembles an error function in good agreement with experiment [7]. As expected, with increasing flow rate the response time is shifted to shorter times, decreasing from 600 ms for no flow to 50 ms for the fastest flow (where defined as a threshold t_{90} = 90% of the steady state level).

This behavior depends sensitively on device length and height. For example, as illustrated in Fig. 5b, a ten times longer and four times shallower sensor with an increased adsorption of $\varepsilon = 0.2$ yields qualitative transient shapes that are largely unchanged, but the overall response time is lengthened considerably. It specifically is increased to t_{90} = 15 s for the diffusive case and is reduced down to 1.8 s by fast flow.

The very dominant influence of the dynamic adsorption on the transient response is depicted in Fig. 5c for the standard geometry and a flow rate of 75 µm/s. Here the fraction of adsorption is varied from $\varepsilon = 0.1$–5 showing a substantial increase in the time response for strong adsorption.[4]

Three sets of exemplary transport parameters are summarized in Table 1.

Table 1
Three examples of device and transport parameters.

	Diffusive coupling	Advective flow	Long, shallow nanochannel
Width w	5 µm	5 µm	5 µm
Length L	10 µm	10 µm	100 µm
Height h	200 nm	200 nm	50 nm
Pressure Δp	0	3 kPa	50 kPa
Flow rate Q	0	60 pL/min	1.5 pL/min
Velocity U	0	1000 µm/s	100µm/s
$\varepsilon = N_{sol}/N_{ads}$	1	1	0.2
U_{eff}	0	500 µm/s	17 µm/s
Reactivity k_0	5 cm/s	5 cm/s	5 cm/s
Diffusivity D	5×10^{-10} m^2/s	5×10^{-10} m^2/s	5×10^{-10}m^2/s
Re = $\rho U h/\eta$	–	2×10^{-4}	5×10^{-6}
Pe = Uh/D	–	0.4	0.01
Gz = Pe h/L	–	0.008	5×10^{-6}
Da = $k_0 h/D$	20	20	5
Response t_{90}	0.6 s	0.05 s	9 s

5. Fast flow regime

All of the cases discussed above have in common that an identical limiting current is reached under steady state conditions independently of the flow velocity. This intrinsic advantage of nanogap transducers as compared to ultramicroelectrodes [3,4] is therefore not only due to the high hydraulic resistances of the devices [5], but is more fundamentally caused by the device operating in the regime of very low Graetz numbers. That is, due to the high aspect ratio, molecular transport *across* the nanochannel and thereby the detected faradaic current is always limited by diffusion exclusively—even when longitudinal advection is superimposed on this motion.

The finite element simulation further allows investigating of a regime of fast flow in which this typical behavior is changed. In Fig. 6, the concentrations c_{red} and c_{ox} are shown for the

[4] All responses in Fig. 5c are normalized to zero at $t = 0$ to facilitate comparison.

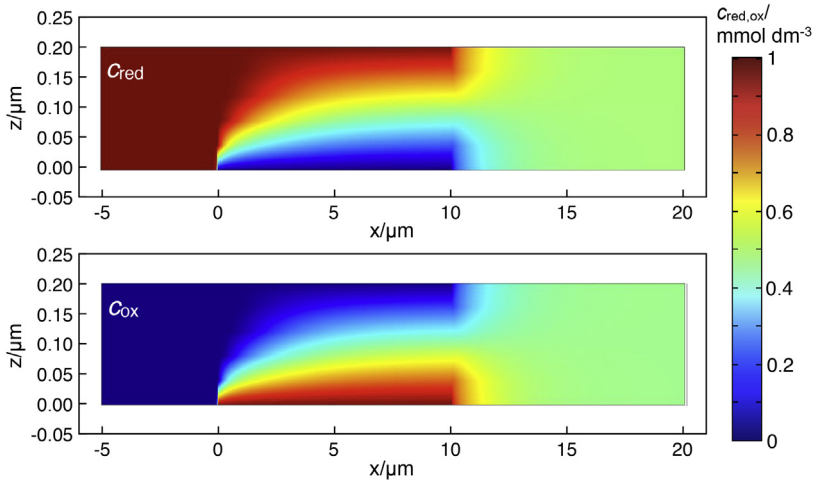

Fig. 6. Simulated breakdown of the diffusion dominated regime at a fast flow velocity of 0.25 m/s. At this comparatively large Graetz number Gz = 0.2, c_{red} and c_{ox} are no longer distributed homogeneously along the device.

standard device geometry but a fast inlet advection of $U = 0.25$ m/s (thus approximately three orders of magnitude faster than the flows considered above). Here, the analyte distributions are no longer homogeneous along the longitudinal x-direction: reduced molecules are transported into the device so fast that not all of them have a chance to impinge on the bottom electrode and get oxidized immediately. Correspondingly, the concentration profiles are neither linear across nor constant along the sensor anymore, and the limiting current does decrease with increasing flow rate. This fast flow corresponds to a regime of Pe = 100 and Gz = 0.2 (while the liquid flow is still laminar at Re = 0.05).

This new regime would however be difficult to access experimentally. For the parameters employed above, an unrealistically high pressure of 7.5 bar would be needed to drive the flow, which is difficult to achieve without mechanical breakdown or leakage of the transducer.

6. Conclusions

We have introduced a continuum mass transfer model for reversible redox couples in nanofluidic electrochemical sensors and used it to investigate the transient response of these transducers in the presence of surface adsorption. The model predicts that it is possible to decrease the response time considerably by actively transporting the analyte into the device by pressure-driven flow instead of relying on diffusive equilibration. Given a maximum experimentally realizable flow rate, the response time is ultimately limited by dynamic adsorption.

From a more fundamental perspective, we note that a fit of experimental data to simulated numerical transients should make it possible in the future to independently extract parameters such as adsorption and the flow rate from the measured current time traces. Such experiments are currently in the planning stage in our laboratory.

Finally, we note that the model can be straightforwardly extended to include additional aspects, in particular: different diffusion coefficients of the ox- and red-species of a redox couple [20]; electrical migration of analyte molecules in the absence of supporting electrolyte; more complex geometries with multiple detectors in one nanochannel [8]; bulk reactions in the sensor; and explicit inclusion of electrode kinetic effects.

Acknowledgements

We gratefully acknowledge financial support from the Netherlands Organization for Scientific Research (NWO) and the European Research Council (ERC).

Appendix A. Supplementary data

Supplementary data associated with this article can be found, in the online version, at http://dx.doi.org/10.1016/j.electacta.2013.05.142.

References

[1] C. Batchelor-McAuley, E.J.F. Dickinson, N.V. Rees, K.E. Toghill, R.G. Compton, New electrochemical methods, Analytical Chemistry 84 (2012) 669.
[2] M.A.G. Zevenbergen, P.S. Singh, E.D. Goluch, B.L. Wolfrum, S.G. Lemay, Stochastic sensing of single molecules in a nanofluidic electrochemical device, Nano Letters 11 (2011) 2881.
[3] A.C. Fisher, R.G. Compton, Chronoamperometry at channel electrodes: a general computational approach, Journal of Physical Chemistry 95 (1991) 7538.
[4] A.C. Fisher, C.W. Davies, Q. Fulian, M. Walters, Hydrodynamic microelectrodes: the microdisk electrode: theory and experiment, Electroanalysis 9 (1997) 849.
[5] L. Rassaei, K. Mathwig, E.D. Golluch, S.G. Lemay, Hydrodynamic voltammetry with nanogap electrodes, Journal of Physical Chemistry C 116 (2012) 10913.
[6] P.S. Singh, H.-S.M. Chan, S. Kang, S.G. Lemay, Stochastic amperometric fluctuations as a probe for dynamic adsorption in nanofluidic electrochemical systems, Journal of the American Chemical Society 133 (2011) 18289.
[7] S. Kang, K. Mathwig, S.G. Lemay, Response time of nanofluidic electrochemical sensors, Lab on a Chip 12 (2012) 1262.
[8] K. Mathwig, D. Mampallil, S. Kang, S.G. Lemay, Electrical cross-correlation spectroscopy; measuring picoliter-per-minute flows in nanochannels, Physical Review Letters 109 (2012) 118302.
[9] K. Mathwig, S.G. Lemay, Pushing the limits of electrical detection of ultralow flows in nanofluidic channels, Micromachines 4 (2013) 138.
[10] T. Gervais, K.F. Jensen, Mass transport and surface reactions in microfluidic systems, Chemical Engineering Science 61 (2006) 1102.
[11] M.A.G. Zevenbergen, P.S. Singh, E.D. Goluch, B.L. Wolfrum, S.G. Lemay, Electrochemical correlation spectroscopy in nanofluidic cavities, Analytical Chemistry 81 (2009) 8203.
[12] P.S. Singh, E. Kätelhön, K. Mathwig, B. Wolfrum, S.G. Lemay, Stochasticity in single-molecule nanoelectrochemistry: origins, consequences, and solutions, ACS Nano 6 (2012) 9662.
[13] R.B. Schoch, L.H. Cheow, J. Han, Electrical detection of fast reaction kinetics in nanochannels with an induced flow, Nano Letters 7 (2007) 3895.
[14] R. Karnik, K. Castelino, R. Fan, P. Yang, A. Majumdar, Effect of biological reactions and modifications on conductance of nanofluidic channels, Nano Letters 5 (2005) 1638.

[15] M.A.G. Zevenbergen, B.L. Wolfrum, E.G. Goluch, P.S. Singh, S.G. Lemay, Fast electron-transfer kinetics probed in nanofluidic channels, Journal of the American Chemical Society 131 (2009) 11471.
[16] P. Sun, M.V. Mirkin, Kinetics of electron-transfer reactions at nanoelectrodes, Analytical Chemistry 78 (2006) 6526.
[17] J.J. Watkins, J. Chen, H.S. White, H.D. Abruña, E. Maisonhaute, C. Amatore, Zeptomole voltammetric detection and electron-transfer rate measurements using platinum electrodes of nanometer dimensions, Analytical Chemistry 75 (2003) 3962.
[18] H. Bruus, Theoretical Microfluidics, Oxford University Press, Oxford, 2008.
[19] L.B. Anderson, C.N. Reilley, Thin-layer electrochemistry: steady-state methods of studying rate processes, Journal of Electroanalytical Chemistry 10 (1965) 295.
[20] D. Mampallil, K. Mathwig, S. Kang, S.G. Lemay, Redox couples with unequal diffusion coefficients: effect on redox cycling, Analytical Chemistry 85 (2013) 6053.